Stabilization of Amide-Based Complexes of Niobium and Tantalum Using Malonates as Chelating Ligands: Precursor Chemistry and Thin Film Deposition

Malte Hellwig,[†] Andrian Milanov,[†] Davide Barreca,[‡] Jean-Laurent Deborde,[§] Reji Thomas,[⊥] Manuela Winter,[†] Ulrich Kunze,[§] Roland A. Fischer,[†] and Anjana Devi*[,†]

Inorganic Materials Chemistry Group, Lehrstuhl für Anorganische Chemie II, Ruhr-University Bochum, 44801 Bochum, Germany; ISTM-CNR and INSTM, Department of Chemistry, Padova University, Via Marzolo, 1, 35131 Padova, Italy; Institute for Electronic Materials and Nanoelectronics, Ruhr-University Bochum, 44801 Bochum, Germany; and IFF-Institut für Festkörperforschung and CNI-Center for Nanoelectronic Systems for Information Technology, Forschungszentrum Jülich, 52425 Jülich, Germany

Received December 21, 2006. Revised Manuscript Received August 30, 2007

The stabilization of the reactive amide complexes of niobium and tantalum with malonates as chelating ligands leads to stable six-coordinated monomeric complexes ([M(NMe$_2$)$_4$(dbml)]; M = Nb, Ta), namely tetrakis(dimethylamido)(di-*tert*-butylmalonato)niobium(V) (**1**) and tetrakis(dimethylamido)(di-*tert*-butylmalonato)tantalum(V) (**2**). Compounds **1** and **2** were characterized by ^{1}H NMR, ^{13}C NMR, EI-mass spectroscopy, elemental analysis, and single-crystal X-ray diffraction studies. The thermal properties of the compounds were studied by thermogravimetric analysis. Both the complexes possess good thermal characteristics, improved resistance to air and moisture, and high solubility and stability in solvents compared to their respective parent alkyl amides. Compound **1** was studied for metalorganic chemical vapor deposition (MOCVD) of Nb_2O_5 while compound **2** was studied for liquid injection metalorganic chemical vapor deposition (LI-MOCVD) of Ta_2O_5 thin films. The films were deposited at substrate temperatures from 400 to 800 °C, and for both Nb_2O_5 and Ta_2O_5 the maximum growth rate was at 600 °C. The films were characterized by X-ray diffraction, scanning electron microscopy, and atomic force microscopy for their crystallinity and morphology. Thin film composition was analyzed by X-ray photoelectron spectroscopy, Rutherford backscattering, and depth profiling the composition with secondary neutral mass spectrometry. Electrical properties of the films were studied in terms of the *C*–*V* characteristics.

Introduction

Thin films of functional metal oxides like Nb_2O_5 and Ta_2O_5 have a diverse range of technological applications owing to their interesting electrical and optical properties, for example, as capacitor dielectric materials in dynamic random access memory (DRAM) as well as gate dielectrics for nanoscale complementary metal–oxide–semiconductor (CMOS) devices,[1] for optical and optoelectronic applications such as antireflection coatings in silicon solar cells, electrochromic devices, planar waveguides, etc.[2] In addition, tantalum and niobium oxides are the main components in multicomponent films like strontium bismuth tantalate, $SrBi_2Ta_2O_9$ (SBT), for nonvolatile computer memories, $SrBi_2Nb_2O_9$ (SBN) for nonvolatile ferroelectric memory applications, and Pb(MgNb)O_3 (PMN) and Pb($Sc_{0.5}Ta_{0.5}$)O_3 (PST) for pyroelectric and piezoelectric devices.[3] Ta_2O_5 and Nb_2O_5 have been deposited by several techniques such as sol–gel,[4] metalorganic CVD (MOCVD),[5] pulsed liquid injection MOCVD,[6]

* Corresponding author. E-mail: anjana.devi@rub.de.
† Lehrstuhl für Anorganische Chemie II, Ruhr-University Bochum.
‡ ISTM-CNR.
§ Institute for Electronic Materials and Nanoelectronics, Ruhr-University Bochum.
⊥ IFF-Institut für Festkörperforschung and CNI-Center for Nanoelectronic Systems for Information Technology.

(1) (a) Wilk, G. D.; Wallace, R. M.; Anthony, J. M. *J. Appl. Phys.* **2001**, *89*, 5243. (b) Lee, J. S.; Chang, S. J.; Chen, F.; Sun, S. C.; Liu, C. H.; Liaw, U. H. *Mater. Chem. Phys.* **2003**, *77*, 242. (c) Alers, G. B.; Werder, D. J.; Chabal, Y.; Lu, H. C.; Gusev, E. P.; Garfunkel, T.; Gustafsson, T.; Urdahl, R. S. *Appl. Phys. Lett.* **1998**, *72*, 1187. (d) Yun, J. Y.; Rhee, S. W. *J. Vac. Sci. Technol.* **2000**, *18*, 2822.

(2) (a) Rubio, J. *J. Vac. Sci. Technol.* **1982**, *21*, 1043. (b) Ozer, N.; Lampert, C. M. *J. Sol-Gel Sci. Technol.* **1997**, *8*, 703. (c) Granqvist, C. G. *Handbook of Inorganic Electrochromic Materials*; Elsevier: Amsterdam, 1995. (d) Doumuki, T.; Tamada, H.; Saitoh, M. *Appl. Phys. Lett.* **1994**, *54*, 3533.

(3) (a) Araujo, C. A.; Cuchiaro, J. D.; McMillan, L. D.; Scott, M. C.; Scott, J. F. *Nature (London)* **2002**, *374*, 627. (b) Condorelli, G. G.; Favazza, M.; Bedoya, C.; Baeri, A.; Anastasi, G.; Lo Nigro, R.; Menou, N.; Muller, C.; Lisoni, J. G.; Wouters, D.; Fragala, I. L. *Chem. Mater.* **2006**, *18*, 1016. (c) Ramesh, R.; Aggarwal, S.; Auciello, O. *Mater. Sci. Eng., R* **2001**, 32. (d) Polla, D. L. *Microelectron. Eng.* **1995**, *29*, 51.

(4) (a) Sullivan, B. T.; Clarke, G. A:; Akiyama, T.; Osborne, N.; Ranger, M.; Dobrowolski, J. A.; Howe, L.; Matsumoto, A.; Yizhou, S.; Kikuchi, *Appl. Opt.* **2000**, *39*, 157. (b) Agarwal, G.; Reddy, G. B. *J. Mater. Sci.: Mater. Electron.* **2005**, *16*, 21.

(5) (a) Pollard, K. D.; Puddephatt, R. J. *Chem. Mater.* **1999**, *11*, 1069. (b) Pinzelli, L.; Gros-Jean, M.; Brechet, Y.; Volpi, F.; Bajolet, A.; Giraudin, J. C. *Microlectron. Reliab.* **2007**, *47*, 700. (c) Zeng, W.; Eisenbraun, E.; Frisch, H.; Sullivan, J. J.; Kaloyeros, A. E.; Margalit, J.; Beck, K. *J. Electrochem. Soc.* **2004**, *151*, F172. (d) Li, H.; Dawson, W. A.; Roose, J.; Hoppert, B. D.; Grobe, G.; Leineguth, E. *Chem. Vap. Deposition, Proc. 11th Int. Conf. (EUROCVD-11)* **1997**, 811. (e) Desu, S. B. *Mater. Chem. Phys.* **1992**, *31*, 341.

(6) Porporati, A.; Roitti, S.; Sbaizero, O. *J. Eur. Ceram. Soc.* **2003**, *23*, 247.

(7) (a) Kukli, K.; Ritala, M.; Leskela, M. *Chem. Mater.* **2000**, *12*, 1914. (b) Maeng, W. J.; Park, S.-J.; Kim, H. *J. Vac. Sci. Technol. B* **2006**, *24*, 2276. (c) Maeng, W. J.; Kim, H. *Electrochem. Soc. Solid-State Lett.* **2006**, *9*, G191. (d) Rooth, M.; Kukli, K.; Haarsta, A. *Proc. Electrochem. Soc.* **2005**, *9*, 598.

10.1021/cm0630441 CCC: $37.00 © 2007 American Chemical Society
Published on Web 11/08/2007

atomic layer deposition (ALD),[7] pulsed laser deposition (PLD),[8] and sputtering.[9] The continuing scaling down of device dimension in modern day technology has prompted the use of MOCVD and ALD techniques for growing thin films with precise control of film thickness, defect free films, large area deposition, and conformal coverage on complex or nonplanar device geometries, for example in CMOS applications. An important requirement for the MOCVD process is the availability of precursors with appropriate physical properties and decomposition characteristics. It is also important that the precursors are compatible with each other when used for the growth of multicomponent oxides. In case of precursors where thermal stability as well as incompatibility in terms of thermal decomposition with other precursors (for multicomponent oxides) is a limitation, an alternative route, namely liquid injection MOCVD (LI-MOCVD), could be used. The commonly used precursors for growing Ta and Nb oxides include metal chlorides, metal alkoxides, and mixed metal alkoxide complexes.[10] Metal alkyl amides are another interesting class of precursors for oxide thin film deposition.[11] However, these compounds have limited thermal stability and are highly sensitive to air and moisture, and the instability of metal dialkylamides in solution and upon storage is a cause for concern for LI-MOCVD processes. The alkylamides of Ta and Nb have been used for the MOCVD of TaN and $NbTaO_{(1-x)}N_y$.[12] The Ta amides also have been used for ALD of Ta_2O_5 and TaO_xN_y,[13] but there have been only a couple of reports where metal amides of Ta were used for MOCVD of Ta_2O_5.[14] To our knowledge, there has been no report solely on the MOCVD of Nb_2O_5 using niobium alkylamides, apart from its application for growing $NbTaO_{(1-x)}N_y$ films by MOCVD.[12]

Recently, we have shown that it is possible to tailor the precursor properties of metal alkylamides, and we have been very successful in developing mixed amide complexes of group IV metals. By introducing bulky chelating ligands like malonates[15] and guanidinates,[16] it was possible to tune the precursor characteristics for MOCVD and LI-MOCVD application of group IV oxides. There are reports in literature where the thermal stability of metal alkoxide complexes of Ta and Nb has been improved using chelating ligands,[5a,17] but there has been no report so far on the modification of metal alkyl amide complexes of Ta and Nb to improve its properties. We were motivated to tailor the properties of Ta and Nb alkyl amides as they are interesting for CVD related applications, not only for binary oxides of Nb and Ta but also for multicomponent oxides (SBT, SBN). Our approach was to develop amide-based compounds of Ta and Nb in combination with stabilizing chelating ligands like malonates. This could render higher thermal stability regarding vaporization (N–M–π character), higher stability toward nucleophilic attacks (six-coordinated M center), and low tendency to form dimers (high N–M–π bonding contribution). In addition, the malonate ligands have additional cleavage sites in the molecule (*tert*-butyl groups in the malonate ligands) which could facilitate the easy decomposition of the precursor during a MOCVD process.

In this paper, the synthesis and characterization of two metal amide hybrid complexes of Nb and Ta namely, tetrakis(dimethylamido)(di-*tert*-butylmalonato)niobium(V) (**1**) and tetrakis(dimethylamido)(di-*tert*-butylmalonato)tantalum(V) (**2**) {$[M(NMe_2)_4(dbml)]$; M = Nb (**1**), Ta (**2**)} are discussed. This is the first report on the stabilization of parent alkylamides of Nb and Ta with chelating ligands. The structure and thermal properties of both the compounds are similar. When compared to their respective parent alkylamides, both the complexes exhibit significantly enhanced thermal stability, solubility, and higher stability in solution and are less sensitive to air and moisture. All these features make them attractive both for MOCVD and LI-MOCVD applications. To demonstrate this, the Nb compound was employed for MOCVD and the Ta precursor was used for LI-MOCVD.

Experimental Section

A. General Procedures. All reactions were performed employing a conventional vacuum/argon line using standard Schlenk techniques. Preparation of samples for analysis was carried out in an argon-filled glovebox (MBraun). The solvents were dried and purified by an automatic solvent purification system directly attached to the glovebox (MBraun solvent purification system) and stored

(8) (a) Zhang, J.-Y.; Fang, Q.; Boyd, I. W. *Appl. Surf. Sci.* **1999**, *138–139*, 320. (b) Kinsel, G., Jr. *Microporous Mesoporous Mater.* **1999**, *28*, 111. (c) Sim, H.; Choi, D.; Dongsoo, S.; Lee, S.; Jae-Myong, Y.; Yoo, I.; Hwang, H. *IEEE Electron Device Lett.* **2005**, *26*, 292.

(9) (a) Ezhlilvalavan, S.; Tseng, T. Y. *J. Appl. Phys.* **1998**, *83*, 4797. (b) Wu, A. M.; Wu, P. K.; Rymaszewski, *Appl. Phys. Lett.* **1993**, *62*, 3264. (c) Boughhaba, S.; Islam, M.; McCaffrey, J. P.; Sproule, G. I.; Graham, M. J. *Thin Solid Films* **2000**, *371*, 119. (d) Chaput, F.; Boilot, J.-P. *J. Am. Ceram. Soc.* **1989**, *72*, 1335. (e) Robert, S.; Ryan, J.; Nesbit, L. *J. Electrochem. Soc.* **1986**, *147*, 1405. (f) Chao, N. H.; Kang, H. B.; Kim, Y. H. *Ferroelectrics* **1994**, *152*, 39.

(10) (a) Forsgren, K.; Harsta, A. *Thin Solid Films* **1998**, *343–344*, 111. (b) Kobyakov, V. P. *Inorg. Chem.* **2002**, *38*, 895. (c) Kukli, K.; Ritala, M.; Lesklea, M.; Lappalainen, R. *Chem. Vap. Deposition* **1998**, *4*, 29. (d) Briand, D.; Modnin, G.; Jenny, S.; van der Wal; Jeannret, S.; de Rooij, N.; Banakh, O.; Keppner, H. *Thin Solid Films* **2005**, *493*, 6. (e) Senzaki, Y.; Hochberg, A.; Norman, J. *Adv. Mater. Opt. Electron.* **2000**, *10*, 93.

(11) (a) Chiu, H. T.; Wang, C. N.; Chaung, S. H. *Chem. Vap. Deposition* **2000**, *6*, 223. (b) Hausmann, D. M.; Rouffignac, P.; Smith, A.; Gordon, R. G.; Monsma, D. *Thin Solid Films* **2003**, *443*, 1. (c) Bailey, P. J.; Pace, S. *Coord. Chem. Rev.* **2001**, *214*, 91. (d) Machida, H.; Hoshino; Suzuki, T.; Ogura, A.; Oshita, Y. *J. Cryst. Growth* **2002**, *237*, 586.

(12) (a) Liu, X. L.; Babock, R.; Lane, A. M.; Belot, J. A.; Ott, W. A.; Metz, V. M.; Kannenwurf, C. R.; Chang, P. H. R.; Marks, T. J. *Chem. Vap. Deposition* **2001**, *7*, 25. (b) Gau, W. C.; Wu, C. W.; Chang, T. C.; Liu, P. T.; Chu, C. J.; Chen, C. H.; Chen, L. J. *Thin Solid Films* **2002**, *420–421*, 548.

(13) (a) Maeng, W. J.; Park, S. J.; Kim, H. *J. Vac. Sci. Technol. B* **2006**, *24*, 2276. (b) Maeng, W. J.; Kim, H. *Electrochem. Solid State Lett.* **2006**, *9*, G191. (d) Maeng, W. J.; Lim, S. J.; Kwon, S. J.; Kim, H. *Appl. Phys. Lett.* **2007**, *90*, 062009.

(14) (a) Son, K. A.; Mao, A. Y.; Sun, Y. M.; Kim, Y.; Liu, F.; Kamath, A. *Appl. Phys. Lett.* **1998**, *72*, 1187. (b) Chiu, H. T.; Wang, C. N.; Chaung, S. H. *Chem. Vap. Deposition* **2000**, *6* (5), 223. (c) Pinzelli, L.; Gros-Jean, M.; Brechet, Y.; Volpi, F.; Bajolet, A.; Giraudinm, J. C. *Microelectron. Reliab.* **2007**, *47*, 700.

(15) (a) Thomas, R.; Milanov, A.; Bhakta, R.; Patil, R.; Winter, M.; Ehrhart, P.; Waser, R.; Devi, A. *Chem. Vap. Deposition* **2006**, *12*, 295. (b) Milanov, A.; Bhakta, R.; Thomas, R.; Ehrhart, P.; Winter, M.; Waser, R.; Devi, A. *J. Mater. Chem.* **2006**, *16*, 437.

(16) (a) Milanov, A.; Bhakta, R.; Baunemann, A.; Becker, H.-W.; Thomas, R.; Ehrhart, P.; Winter, M.; Devi, A. *Inorg. Chem.* **2006**, *45*, 11008. (b) Devi, A.; Bhakta, R.; Milanov, R.; Hellwig, M.; Barreca, D.; Tondello, E.; Thomas, R.; Ehrhart, P.; Winter, M.; Fischer, R. A. *Dalton Trans.* **2007**, *17*, 1671.

(17) (a) Williams, P. A.; Jones, A. C.; Wright, P. J.; Crosbie, M. J.; Bickley, J. F.; Steiner, A.; Davies, H. O.; Leedham, T. J. *Chem. Vap. Deposition* **2002**, *8*, 110. (b) Lim, S.; Lee, J. C.; Sohn, S.; Lee, W. I.; Lee, I. *Chem. Mater.* **2002**, *14*, 1548.

Table 1. Crystal Data and Structure Refinement for $[Nb(NMe_2)_4(dbml)]$ (1) and $[Ta(NMe_2)_4(dbml)]$(2)

empirical formula	$C_{38}H_{86}N_8O_8Nb_2$	$C_{38}H_{86}N_8O_8Ta_2$
molecular weight	968.97	1145.05
temperature (K)	108(2)	105(2)
wavelength Mo Kα (Å)	0.71073	0.71073
crystal size (mm)	0.15 × 0.11 × 0.05	0.14 × 0.09 × 0.02
crystal system, space group	triclinic, $P\bar{1}$	triclinic, $P\bar{1}$
a (Å)	11.146(3)	11.1480(12)
b (Å)	14.675(4)	14.6795(13)
c (Å)	17.093(5)	17.1086(15)
α (deg)	112.97(3)	112.819(8)
β (deg)	95.36(2))	94.993(8)
γ (deg)	96.01(2)	96.253(8)
cell volume (Å^3)/Z	2532.4(12)/2	2539.6(4)/2
density δ_{calc} (g cm^{-3})	1.271	1.497
absorption coefficient μ (mm^{-1})	0.503	0.282
F (000)	1032	1160
θ range for data collection (deg)	3.20–25.00	3.14–27.56
completeness to θ = 25.00° [%]	99.4	99.0
index ranges	$13 \leq h \leq 13, -17 \leq k \leq 17, -20 \leq l \leq 20$	$14 \leq h \leq 14, -19 \leq k \leq 19, -22 \leq l \leq 22$
reflexes collected/ unique	31108/8873 [R(int) = 0.0608]	44623/11611 [R(int) = 0.0869]
reflexes observed	6573 $F_0 > 4\sigma(F_0)$	7531 $F_0 > 4\sigma(F_0)$
refinement method	full-matrix least-squares on F^2	full-matrix least-squares on F^2
data/restraints/parameters	8873/0/505	11611/0/533
goodness-of-fit on F^2 (GOF)	1.040	0.912
final R indices [$I > 2\sigma(I)$]	$R1 = 0.0479$, $wR2 = 0.1331$	$R1 = 0.0446$, $wR2 = 0.0876$
R indices (all data)	$R1 = 0.0703$, $wR2 = 0.1418$	$R1 = 0.0767$, $wR2 = 0.0967$
largest difference peak and hole (e Å^{-3})	0.715 and −0.802	4.394 and −2.175

over molecular sieves (4 Å). The NMR solvents were degassed and dried over activated molecular sieves. The Nb and Ta amide starting compounds, namely pentakis(dimethylamido)niobium (PDMAN) $[Nb(NMe_2)_5]$ and pentakis(dimethylamido)tantalum (PDMAT) $[Ta(NMe_2)_5]$, were synthesized following literature reported procedures[18] while di-*tert*-butyl malonate (>98%, Aldrich) was used as received.

Single crystals of compounds **1** and **2** were mounted on thin glass capillaries and then cooled to data collection temperature (150 K). Diffraction data were collected on an Oxford X-calibur 2 diffractometer using graphite monochromated Mo Kα radiation (λ = 0.710 73 Å). All structures were solved by direct methods using the SHELXL-97 software package and refined by full matrix least-squares methods based on F^2 with all observed reflections. Final agreement factors are listed in Table 1.

^{1}H and ^{13}C NMR spectra were recorded either on the Bruker Advance DRX 400 or on the Bruker Advance DPX 250 spectrometer. Elemental analysis was performed using a CHNSO Vario EL instrument. Electronic ionization (EI) mass spectra were recorded using a Varian MAT spectrometer supplied with an ionizing energy of 70 eV. Melting points were measured in sealed capillaries under Ar and are uncorrected. Thermogravimetric analysis (TGA) was performed using a Seiko TG/DTA 6300S11 instrument (sample size ~10 mg), with a heating rate of 5 °C/min. All measurements were performed under atmospheric pressure in the temperature range of 20–600 °C under flowing high-purity (99.9999%) nitrogen atmosphere (flow rate of 300 mL/min). For isothermal studies, the precursor was heated to a set temperature and maintained at that temperature for a couple of hours.

B. Synthesis of Nb and Ta Precursors. *Synthesis of tetrakis-(dimethylamido)(di-tert-butylmalonato)niobium(V) $[Nb(NMe_2)_4(dbml)]$ (***1***)*: A solution of 0.72 g of (2.3 mmol) pentakis(dimethylamido)niobium (PDMAN) $[Nb(NMe_2)_5]$ in 20 mL of hexane was stirred at room temperature. To this 0.57 mL of Hdbml (0.55 g, 2.5 mmol) diluted in 20 mL of hexane was added dropwise. After stirring the mixture for 24 h, the solution was cooled to −20 °C. The product crystallizes in the form of red crystals. Yield (based on $Nb(NMe_2)_5$): 18.5 g (32.34 mmol, ~94%); melting point: 93 °C. EA$_{calc}$: C: 47.10%, H: 8.95%, N: 11.56%; Found: C: 46.92%, H: 8.84%, N: 11.32%. EI(70 eV) m/z = 484 [M$^+$, <1%], 440 [M$^+$ – NMe$_2$, 21%], 328 [M$^+$ – NMe$_2$ – 2× isobutene, 7%], 225 [M$^+$ – NMe$_2$ – dbml, 62%], 161 [M$^+$ − 4× NMe$_2$ – 2× ^{t}Bu, 100%]. ^{1}H NMR (400 MHz, C_6D_6, RT) δ [ppm] = 4.91 [1 H, Nb–O–C(OC(CH$_3$)$_3$C**H**–)]; 3.58, 3.40 [24H, Nb(N(C**H**$_3$)$_2$]; 1.60 [18H, Nb–O–C(OC(C**H**$_3$)$_3$)CH–)]. ^{13}C NMR (400 MHz, C_6D_6, RT) δ [ppm] = 174.85 [Nb–O–**C**(OC(CH$_3$)$_3$)CH–)]; 78.43 [Nb–O–C–(O**C**(CH$_3$)$_3$)CH–)]; 70.72 [Nb–O–C–(OC(CH$_3$)$_3$)**C**H–)]; 48.70, 46.91 [Nb(N(**C**H$_3$)$_2$]; 29.25 [Nb–O–C–(OC(**C**H$_3$)$_3$)CH–)].

*Synthesis of Tetrakis(dimethylamido)(di-tert-butylmalonato)tantalum(V) $[Ta(NMe_2)_4(dbml)]$ (***2***):* The preparation of compound **2** follows the synthesis route adopted for compound **1**. Instead of $[Nb(NMe_2)_5]$ as the metal-containing compound, pentakis(dimethylamido)tantalum, PDMAT $[Ta(NMe_2)_5]$ (13.75 g, 34.29 mmol), dissolved in 100 mL of hexane was used for the synthesis. To this, a solution of 8.5 mL (8.16 g, 37.7 mmol) of Hdbml was added dropwise. The mixture was stirred at room temperature for 24 h and cooled to −20 °C, resulting in yellow crystals. Yield (based on $Ta(NMe_2)_5$): 18.5 g (32.34 mmol, ~94%); melting point: 116 °C. EA$_{calc}$: C: 39.86%, H: 7,57%, N: 9.79%. Found: C: 39.60%, H: 7.66%, N: 9.49%. EI(70 eV) m/z = 572 [M$^+$, 3%], 528 [M$^+$ – NMe$_2$, 66%], 472 [M$^+$ – NMe$_2$ – isobutene, 12%], 416 [M$^+$ – NMe$_2$ – 2× isobutene, 58%], 398 [M$^+$ − 4× NMe$_2$, 14%], 357 [M$^+$ – dbml, 7%], 330 [M$^+$ − 3× NMe$_2$ –2× isobutene, 100%], 281 [M$^+$ − 3× NMe$_2$ – 2× isobutene – CO$_2$, 13%]. ^{1}H NMR (400 MHz, C_6D_6, RT) δ [ppm] = 4.92 [1 H, Ta–O–C(OC(CH$_3$)$_3$)C**H–**)]; 3.72, 3.54 [24H, Ta(N(C**H**$_3$)$_2$]; 1.58 [18H, Ta–O–C(OC (C**H**$_3$)$_3$)CH–)]. ^{13}C NMR (400 MHz, C_6D_6, RT) δ [ppm] = 175.0 [Ta–O–**C**(OC(CH$_3$)$_3$)CH–)]; 79.2 [Ta–O–C–(O**C**(CH$_3$)$_3$)CH–)]; 71.5 [Ta–O–C–(OC(CH$_3$)$_3$)**C**H–)]; 47.2, 45.5 [Ta(N(**C**H$_3$)$_2$]; 29.1 [Ta–O–C–(OC(**C**H$_3$)$_3$)CH–)].

C. Thin Film Deposition. A cold wall horizontal MOCVD system[19] operating under reduced pressure was used for thin film deposition. The depositions were carried out on Si(100) substrates (1 cm × 1 cm). Prior to deposition, the substrates were ultrasonically cleaned in acetone and propanol, rinsed with deionized water, and dried with nitrogen. High-purity nitrogen (99.9999%, 50 sccm) was

(18) Bradley, D. C.; Thomas, I. M. *Can. J. Chem.* **1962**, *40*, 449.

(19) Devi, A.; Rogge, W.; Wohlfart, A.; Hipler, F.; Becker, H. W.; Fischer, R. A. *Chem. Vap. Deposition* **2000**, *6*, 245.

Scheme 1. Synthesis of Malonate Complexes Using Amide Route (M = Nb, Ta)

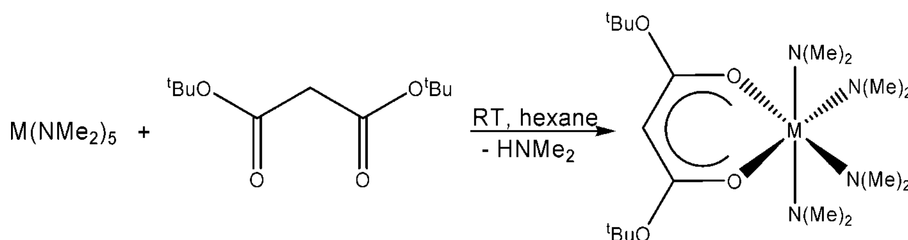

used as the carrier gas and oxygen (99.998%, 50 sccm) as the oxidant, and the flow rates were controlled using mass flow controllers (MKS). About 100 mg of the precursor was used for each deposition, and the precursor vaporizer was maintained at 100 °C for both the compounds. The films were deposited at 5 mbar reactor pressure over the temperature range 400–800 °C. The LI-MOCVD of Ta_2O_5 thin films on Si(100) substrates was carried out in an Aixtron AIX-200FE reactor. The Ta precursor was dissolved in hexane (0.05 M solution). This was then injected by a TRIJET system with a typical pulse length of 0.8 ms (corresponding to 5 μL precursor solution per pulse) and a pulse frequency of 1 Hz. The vaporizer temperature was set to 200 °C, and all the depositions were carried out at a reactor pressure of 5 mbar. High-purity nitrogen was used as the carrier gas (1000 sccm) with an additional flow of oxygen (400 sccm) acting as the oxidizing agent. The deposition temperature was varied in the temperature range 400–700 °C.

D. Film Characterization. XRD analysis of the films was carried out in a Bruker AXS D8 Advance diffractometer, using Cu Kα radiation (1.5418 Å). Surface morphology was studied with SEM (LEO (Zeiss) and AFM (Nanoscope Multimode III AFM; Digital Instruments). Film composition was determined by X-ray photoelectron spectroscopy (XPS), Rutherford backscattering (RBS), and secondary neutral mass spectrometry (SNMS) analysis. The XPS spectra were recorded on a Perkin-Elmer Φ 5600ci spectrometer at a pressure lower than 10^{-9} mbar, using a monochromatized Al Kα excitation source (1486.6 eV). The spectrometer was calibrated by assigning to the Au $4f_{7/2}$ line the binding energy (BE) of 84.0 eV with respect to the Fermi level. The BE shifts were corrected assigning to the C 1s line of adventitious carbon a value of 284.8 eV. The estimated standard deviation for BEs was ±0.2 eV. The atomic compositions were evaluated using sensitivity factors provided by Φ V5.4A software. Ar^+ sputtering was carried out at 3 kV and 0.5 mA cm^{-2} beam current density, with an argon partial pressure of 5×10^{-8} mbar. The sample was introduced directly into the analysis chamber by a fast entry lock system. RBS measurements were performed using an instrument from the Dynamitron Tandem Laboratory (DTL) in Bochum. A beam intensity of about 20 nA incident to the sample perpendicular to the surface was used. The backscattered particles were measured at an angle of 170° by a Si detector with a resolution of 16 keV. The stoichiometry of the films was calculated using the program RBX,[20] and new values for the stopping power of Nb and Ta[21] have been used. The composition of the films was determined by depth-profiling using SNMS measurements employing a VG SIMSLABB IIIA instrument [MATS (UK) Ltd.]. The primary ion beam was argon at 10 keV, usually operated at high currents (0.8–1.0 μA) over large areas (0.5–4 mm raster size) depending on the total depth requirements. For electrical measurements, the deposition of the Pt top electrode was done by sputtering and patterning by lift-off process. The thickness of the films used for this study was around 265 nm for Nb_2O_5 and 220 nm for Ta_2O_5, and the area of the top electrode was 0.0491 mm^2. Capacitance–voltage (*C*–*V*) characteristics of the MIS structures were obtained using a HP4284 LCR meter at a frequency of 100 kHz by sweeping the voltage from inversion to accumulation and back.

Results and Discussion

Precursor Synthesis, Spectroscopic, and Structural Characterization. The synthetic approach involves the direct reaction of 1 equiv of ligand Hdbml with niobium dimethyl amide or tantalum dimethyl amide complexes in *n*-hexane (Scheme 1). These protolytic ligand exchange reactions proceed easily at room temperature observable through the color change from light red into deep red for complex **1** and from pale yellow into dark yellow for complex **2**. The resulting complexes were purified by recrystallization from hexane at −20 °C. Efforts to replace more than one amide moiety were not successful, which can be attributed to two factors, viz. steric hindrance and/or complete saturation of coordination sphere of the metal center. These observations are in consistence with alkoxide–β-diketonate complexes of Nb and Ta.[17a] Compounds **1** and **2** were crystallized as needle-shaped crystals, and the complexes were mononuclear containing four dimethylamido groups and one bidentate chelating di-*tert*-butyl malonate moiety (Figure 1a,b). Since both the compounds display similar structural properties, we describe in detail only the solid state structure of compound **1**. The crystallographic data for both the compounds are given in Table 1.

The compound $[Nb(NMe_2)_4(dbml)]$ (**1**) crystallizes in the triclinic space group $P\bar{1}$. A representation of the molecule with the atomic numbering scheme is shown in Figure 1a. Each unit cell has two monomeric molecules wherein the niobium metal center is coordinated by four dimethylamido groups and one chelating dbml ligand in a distorted octahedral geometry. The nitrogen atoms N(11) and N(12) form an equatorial plane with the oxygen atoms of the dbml ligand. Axial positions can be defined by the bonds Nb(1)–N(13) and Nb(1)–N(14). The Nb–N bond length can be divided into two classes, in which the Nb–N bond length of the dbml trans directed dimethylamido groups ((Nb(1)–N(12) and Nb(1)–N(11)) are about 0.02 Å shorter than the others, possibly due to slightly stronger π-donating properties of the amido groups compared to the dbml ligand. Each dimethylamido ligand can be regarded as four-electron donor, shown by the relatively short Nb–N bond length (Table 2). The sum of the angles C(143)–N(12)–C(132)/C(143)–N(12)–Nb(1)/C(132)–N(12)–Nb(1) is 359.9°, indicating sp^2-hybridized nature of nitrogen in the complex. The Nb–O bond lengths

(20) Kótai, E. *Nucl. Instrum. Methods* **1994**, *B85*, 588.
(21) Baving, P.; Becker, H. W.; Rolfs, C.; Zabel, H. *Nucl. Instrum. Methods* **2002**, *B194*, 363–368.

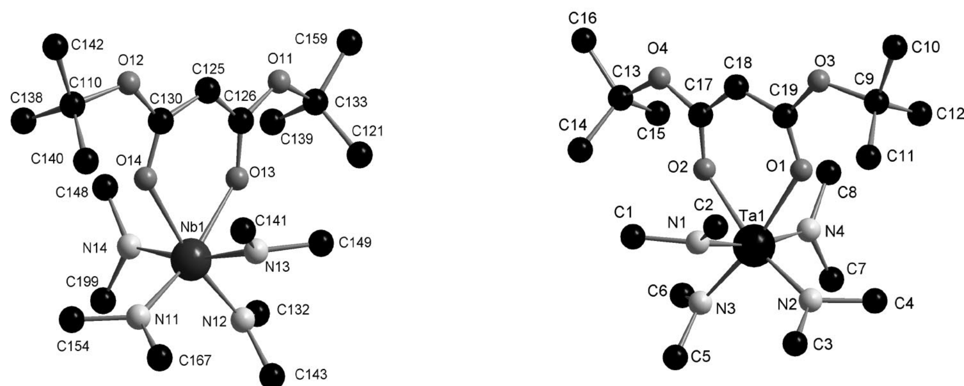

Figure 1. Molecular structure of (a) $[Nb(NMe_2)_4(dbml)]$ (**1**) and (b) $[Ta(NMe_2)_4(dbml)]$ (**2**) in the solid state. (For reasons of clarity all atoms in the figure are shown without thermal ellipsoids.)

Table 2. Selected Bond Lengths (Å) and Angles (deg) for Compounds 1 and 2

Bond Lengths (Å) for $[Nb(NMe_2)_4(dbml)]$ (**1**)			
Nb(1)–N(12)	1.987(4)	Nb(1)–N(13)	2.028(4)
Nb(1)–N(11)	2.007(4)	Nb(1)–O(14)	2.178(3)
Nb(1)–N(14)	2.027(4)	Nb(1)–O(13)	2.194(3)
Bond Angles (deg)			
O(14)–Nb(1)–O(13)	78.08(11)	N(13)–Nb(1)–N(14)	167.07(15)
N(12)–Nb(1)–O(14)	168.33(14)	N(12)–Nb(1)–N(11)	103.74(16)
Bond Lengths (Å) for $[Ta(NMe_2)_4(dbml)]$ (**2**)			
Ta(1)–O(1)	2.170(4)	Ta(1)–N(3)	2.000(5)
Ta(1)–O(2)	2.175(4)	Ta(1)–N(1)	2.039(5)
Ta(1)–N(2)	1.990(5)	Ta(1)–N(4)	2.043(5)
Bond Angles (deg)			
O(1)–Ta(1)–O(2)	78.25(15)	N(2)–Ta(1)–O(2)	166.07(19)
N(2)–Ta(1)–N(3)	103.5(2)	N(1)–Ta(1)–N(4)	90.66(19)

are found to be 2.178(3) Å for Nb(1)–O(14) and 2.194(3) Å for Nb(1)–O(13). Compared to the Nb–O bond length of the dbm ligand of $[Nb(OEt)_4(dbm)]$,[17a] compound **1** shows longer bond lengths (2.129 and 2.123 Å). This is an evidence for the *trans* influence of the dimethylamido ligands which causes a lengthening of the Nb–O bonds directed in opposite directions. The distorted octahedral geometry is identifiable through the small bite angle of 78.08° ((O(14)–Nb(1)–O(13)) for malonates.[15] A significant deviation is observed in the angle between the *trans* located dimethylamido groups and the other dimethylamido ligands. The N(12)–Nb(1)–N(11) angle of 103.74° is about 7–12° larger than the others. Since the bite angle of the malonate ligand is 12° smaller than ideal octahedron, the angle N(12)–Nb(1)–N(11) is fanned out. A distortion of the ideal octahedral geometry is observed from N(13)–Nb(1)–N(14) angle, which is 167°, showing that the axis is bent toward the dbml ligand. As mentioned earlier, the crystallographic data of **2** show a close similarity to compound **1**, and the important characteristic bond lengths and bond angles are given in Table 2.

The NMR study of compound **1** was carried out at room temperature. In the ^1H NMR spectra there are four chemically different protons. This is reasonable through the fact that there are two chemical environments for the amides at the metal center in the compound. Therefore, the amides are symmetrically inequivalent and not exchanging in their positions. In this way, the protons of the amido groups are split into two signals with a chemical shift of $\delta = 3.58$ and 3.40 ppm. The signals at $\delta = 1.60$ ppm can be assigned to the protons of the *tert*-butyl groups and to the proton attached to the methyne carbon atom in central position of the dbml ligand appears at $\delta = 4.91$ ppm. The ^{13}C NMR spectrum confirms the expected structure. The ^1H and ^{13}C NMR spectra for compound **2** taken at room temperature confirm the expected stoichiometry and purity. The spectra show almost identical proton signals like compound **1**, showing a slight shift to low field.

Scheme 2. McLafferty Rearrangement of a Hdbml Ligand in Compound 2 Using EI–Mass Spectrometry

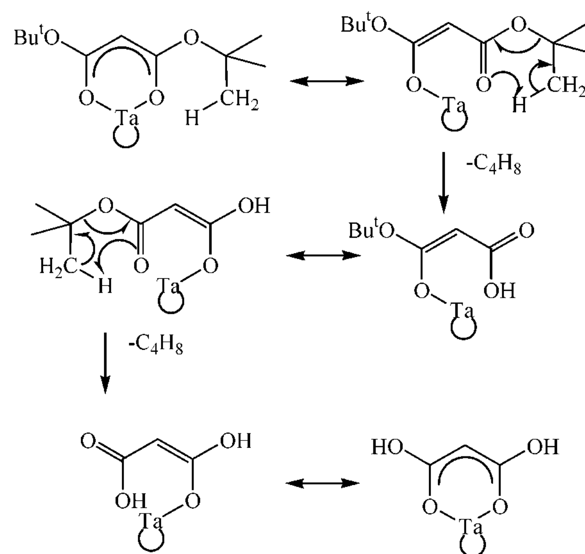

Additional characterization of compounds **1** and **2** were carried out by electronic ionization mass spectrometry (EI-MS) with ionization energy of 70 eV. The molecule ion peak of compound **2** was detected at $m/z = 572$ with an intensity of about 3%. Since no peaks with higher mass were observed, the suggested monomeric structure of **2** could be confirmed. The first fragmentation observed can be assigned to the cleavage of one of the dimethylamido groups ($M^+ - 44$); subsequently the McLafferty rearrangement, typical for esters, takes place identifiable through the mass loss of $m/z = 57$ for isobutene (mechanism shown in Scheme 2). An additional species could be observed at $m/z = 357$. This mass matches with the fragment $[Ta(NMe_2)_4]^+$, which indicates the splitting off of the complete dbml ligand. The base peak at $m/z = 330$ corresponds to the mass of the molecule after the cleavage of three dimethylamido groups and two

Table 3. Overview of the Most Important Fragments Detected by Mass Spectrometry for Nb(NMe$_2$)$_4$(dbml)] (1) and [Ta(NMe$_2$)4(dbml)](2)

fragments	mass and intensity for **1**		mass and intensity for **2**	
	mass [*m*/*z*]	rel int (%)	mass [*m*/*z*]	rel int (%)
M^+ – NMe$_2$	440	21	528	66
M^+ – NMe$_2$ – isobutene			472	12
M^+ – NMe$_2$ – 2×isobutene	328	7	416	58
M^+ – NMe$_2$ – dbml	225	62		
M^+ – 4×NMe$_2$			398	14
M^+ – 4×NMe$_2$ – 2×^{t}Bu	161	100		
M^+ – dbml			357	7
M^+ – 3×NMe$_2$ – 2×isobutene			330	100

isobutene fragments. The fragmentation of the Nb compound (**1**) was similar to that of the Ta compound (**2**). Similar fragmentation pathways were previously reported for the Ti amide malonates.[22] Table 3 gives an overview of the most important fragments that were detected for both the compounds.

Thermal Characterization of Compounds 1 and 2. The thermal characteristics of the newly synthesized Nb and Ta compounds were examined, and Figure 2 shows the comparison of the TG curves of the new Nb and Ta compounds with those of their respective parent alkylamides. It is seen that the substitution of the amide groups with the malonate ligands has certainly an influence on the thermal properties which is evident from the volatility and decomposition characteristics. The compounds are volatile and the onset of volatilization begins at temperatures as low as 50 °C for both the compounds. This is followed by a gradual weight loss as a function of temperature until about 250 and 275 °C, respectively, for the Ta and Nb compounds, beyond which they decompose to leave behind residues of 28% for Nb and 39% for Ta. This shows that there is a good temperature window between volatilization and decomposition for both the compounds. To study the sublimation behavior of the compounds, isothermal studies as a function of time were carried out at atmospheric pressure. It was found that both the precursors sublime with a constant rate over long periods of time (Figure A of the Supporting Information), and from the slope of the curve the sublimation rate was determined. From the thermal studies we can infer that both the new compounds have the necessary requirements such as volatility and sufficient temperature window between volatilization and decomposition to be used as CVD precursors. When comparing the TG curves of the parent alkylamides of Nb and Ta with those of the new compounds, the temperature window of volatilization and decomposition for the pure amides is relatively narrow and, additionally, after decomposition a large residue is left behind, i.e., 47% and 63% for Nb and Ta, respectively.

MOCVD of Nb$_2$O$_5$ and Ta$_2$O$_5$ Thin Films. As mentioned earlier, compound **1** was studied in detail for MOCVD of Nb$_2$O$_5$ and compound **2** was studied in detail for LI-MOCVD of Ta$_2$O$_5$ films. In addition, MOCVD of Ta$_2$O$_5$ was also

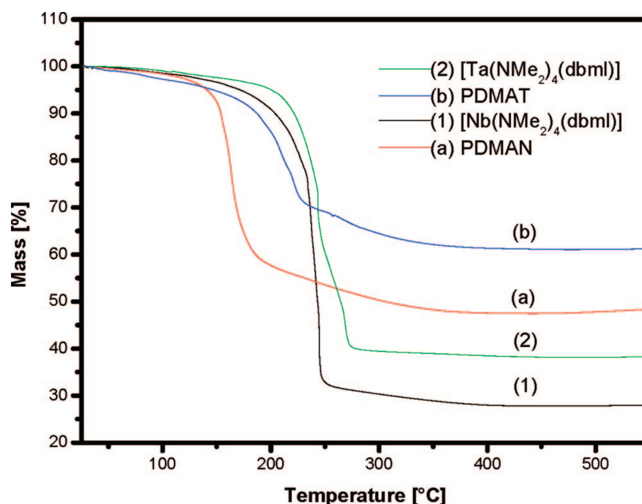

Figure 2. Thermogravimetric analysis of (**1**) [Nb(NMe$_2$)$_4$(dbml)], (**2**) [Ta(NMe$_2$)$_4$(dbml)], (a) PDMAN, and (b) PDMAT.

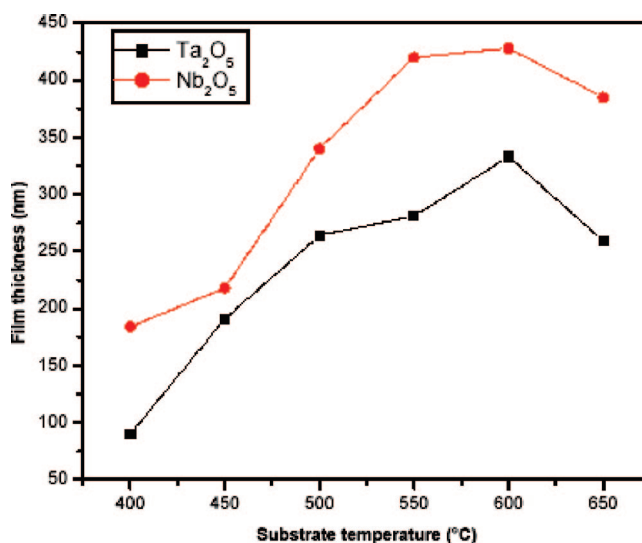

Figure 3. Growth rate as a function of substrate temperature for Nb$_2$O$_5$ thin films using compound **1** grown by MOCVD and Ta$_2$O$_5$ thin films using compound **2** by LI-MOCVD reactor (the curve is just to guide the eye).

performed using compound **2**, although limited experiments were carried out as it was just meant for initial screening of the precursor for film deposition. Some of the characterization data on the MOCVD grown Ta$_2$O$_5$ films are given as Supporting Information. The threshold temperature for growing Nb and Ta oxide films using the newly developed compounds by MOCVD was 400 °C. Even for Ta$_2$O$_5$ films grown by LI-MOCVD, the film growth begins at 400 °C. Figure 3 shows the variation of growth rate as a function of substrate temperature for Nb$_2$O$_5$ films grown by MOCVD and for Ta$_2$O$_5$ films grown by LI-MOCVD. The growth rate steadily increases as a function of substrate temperature, and in each case the maximum growth rate occurs at 600 °C, beyond which the growth rate gradually decreases.

The Nb$_2$O$_5$ films grown by MOCVD from compound **1** were amorphous without any X-ray diffraction features when deposited below 600 °C. The onset of crystallization begins at 600 °C, and polycrystalline films in the orthorhombic phase were formed at higher substrate temperatures (Figure

(22) Baunemann, A.; Hellwig, M.; Varade, A.; Bhakta, R.; Winter, M.; Shivashankar, S. A.; Fischer, R. A.; Devi, A. *Dalton Trans.* **2006**, *28*, 3485.

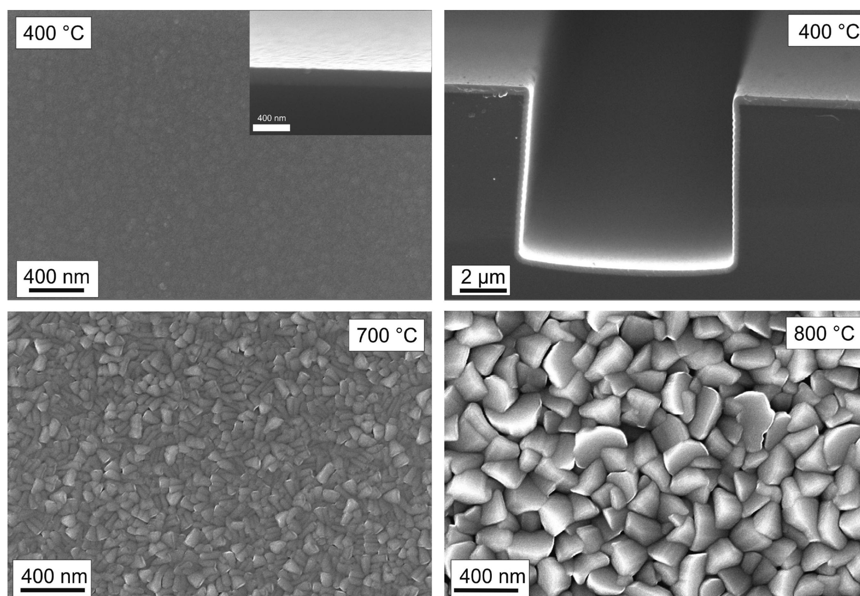

Figure 4. SEM analysis of the Nb_2O_5 thin films grown from compound **1** by thermal CVD on Si(100) at (a) 400 °C and (b) on a patterned substrate at 400 °C, (c) 700 °C, and (d) 800 °C.

B of the Supporting Information). From previous studies it is known that the formation of different Nb_2O_5 phases depends on the film deposition method, annealing temperature, and the precursor used.[23–25] In the case of Ta_2O_5 films grown by MOCVD using compound **2**, X-ray diffraction measurements established that the films were amorphous below 700 °C, as evidenced by the lack of characteristic Ta_2O_5 diffraction peaks. The films begin to crystallize at a slightly higher temperature (above 800 °C) compared to Nb_2O_5 films. The XRD patterns of the as-deposited crystalline films revealed the polycrystalline nature in the orthorhombic phase (β-Ta_2O_5) (Figure B of the Supporting Information). This result is consistent with the other reports in literature where the orthorhombic Ta_2O_5 phase is generally observed for LPCVD deposition of Ta_2O_5.[10d,26] In this study, the Ta_2O_5 films grown by LI-MOCVD using compound **2** were amorphous below 700 °C as in the case of MOCVD grown Ta_2O_5. It was not possible to attain higher substrate temperatures due to the constraint with the heating system associated with the LI-MOCVD reactor.

The surface morphology of the Nb_2O_5 films grown on Si(100) substrates by MOCVD was analyzed by SEM. The SEM images of Nb_2O_5 films deposited at different substrate temperatures are shown in Figure 4. In accordance with the XRD results, the films at lower temperatures are amorphous without any distinct surface features, and the cross section image of the film grown at 400 °C reveals the amorphous nature. At temperatures above 600 °C the films begin to crystallize as seen from the appearance of the grains (at 700 °C). As the substrate temperature is further increased to 800 °C, significant grain growth takes place with well-defined crystallites and grain boundaries. The grain size is of the order of 150–200 nm. Films were also deposited on patterned substrates to study the step coverage (Figure 4b). It is seen that the patterned substrate is uniformly coated with good step coverage. The thickness was of the order of 150 nm on the pattern, 115 nm on the side walls of the trench, and 135 nm in between the two trenches. The surface morphology was also analyzed by AFM, and the surface rms roughness was of the order of 2.2 and 6.3 nm for films grown at 400 and 600 °C, respectively (Figure 5). In the case of MOCVD and LI-MOCVD grown Ta_2O_5 films, the SEM micrographs showed smooth and defect-free surfaces with no distinct surface features. Here, too, the coating of Ta_2O_5 on patterned substrates revealed good step coverage as in the case of Nb_2O_5 films discussed above (Figure C of the Supporting Information). Figure 6 shows the AFM micrographs of the Ta_2O_5 films grown by LI-MOCVD at two different substrate temperatures (400 and 600 °C). Small sharp crystallites can be seen in the 3-dimensional surface plot, and the rms roughness of the film deposited at 400 °C was 0.5 nm while the rms surface roughness increased to 1.7 nm at 600 °C, in which case the film was thicker.

The XPS analyses carried for Nb_2O_5 and Ta_2O_5 films grown at 600 °C are shown in Figures 7 and 8, respectively. The surface analysis revealed the presence of Nb, O, and C for Nb_2O_5 and Ta, O, and C species in the case of Ta_2O_5. Concerning Nb (Figure 7a), the Nb $3d_{5/2}$ BE (207.3 eV) was in good agreement with the values reported for Nb_2O_5,[27,28] and similarly in case of Ta, both Ta $4f_{7/2}$ and Ta $4d_{5/2}$ BEs (26.4 and 230.5 eV, respectively; see Figure 8a) were also in excellent agreement with the literature reported values for

(23) Masse, J.-P.; Szymanowski, Zabbeida, A.; Amassian, A.; Klemberg-Sapieha, J. E.; Martinu, L. *Thin Solid Films* **2006**, *515*, 1674.
(24) Hara, J.; Takahashi, E.; Yoon, J. H.; Sugimoto, K. *J. Electrochem. Soc.* **1994**, *141*, 1669.
(25) O'Neill, S. A.; Parkin, I. P.; Clark, J. H. E.; Mills, A.; Elliott, N. *J. Mater. Chem.* **2003**, *13*, 2952.
(26) Lee, J. S.; Change, J.; Chen, J. F.; Sun, C. H.; Liu, H.; Liaw, U. H. *Mater. Chem. Phys.* **2003**, *77*, 243.
(27) (a) Geyer-Lippmann, J.; Simon, A.; Stollmaier, F. *Z. Anorg. Allg. Chem.* **1984**, *516*, 55. (b) Fontaine, R.; Caillat, R.; Feve, L.; Guittet, M. J. *J. Electron Spectrosc. Relat. Phenom.* **1977**, *10*, 349.
(28) (a) Nefedov, V. I.; Gati, D.; Dzhurinskii, B. F.; Sergushin, N. P.; Salyn, Y. V. *Zh. Neorg. Khim.* **1975**, *20*, 2307. (b) Nefedov, V. I.; Firsov, M. N.; Shaplygin, I. S. *J. Electron Spectrosc. Relat. Phenom.* **1982**, *26*, 65.

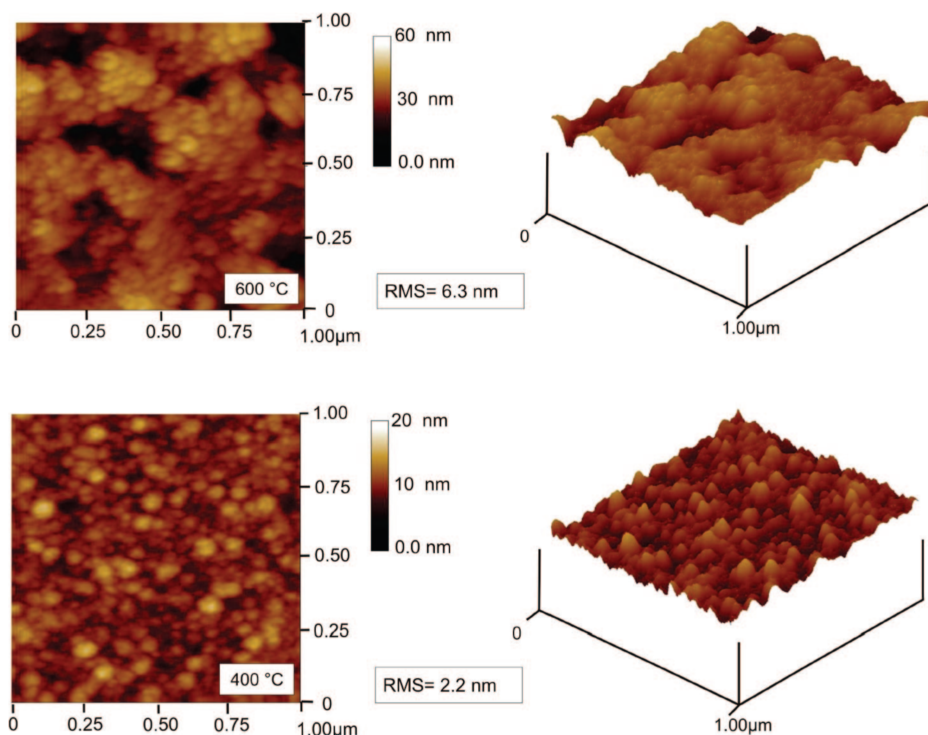

Figure 5. AFM analysis of Nb_2O_5 films grown from compound **1** at 400 and 600 °C by MOCVD.

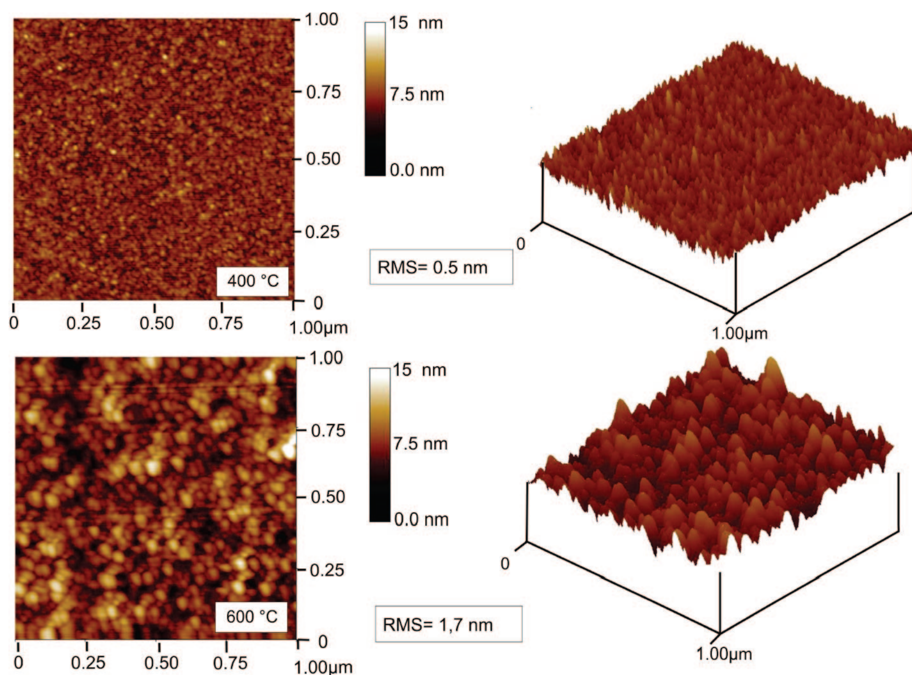

Figure 6. AFM analysis of Ta_2O_5 films grown from compound **2** at 400 and 600 °C by LI-MOCVD.

Ta_2O_5.[29] The surface atomic percentages corresponded to 41.1 and 8.1 at. % for O and Nb in the case of Nb_2O_5 systems and of 48.4 and 9.9 at. % for O and Ta in the case of Ta_2O_5 systems, respectively. Correspondingly, O/Nb and O/Ta ratios in Nb_2O_5 and Ta_2O_5 were both as high as 5, an appreciably greater value with respect to the one expected for stoichiometric Nb_2O_5 or Ta_2O_5. Such a phenomenon could be explained by taking into account the presence of different contributions to the O 1s surface signal. Indeed, the lattice oxygen component in Nb_2O_5 and for Ta_2O_5 was centered at a BE $\approx$ 530.5 eV.[30] In other words, for Nb_2O_5 the major high BE component at $\approx$532.0 eV (Figure 7b) was ascribed to surface –OH groups and underwent an appreciable intensity reduction after sputtering for 10 min. This effect suggested that hydration was limited to the outermost sample

(29) Ho, S. F.; Contarini, S.; Rabalais, J. W. *J. Phys. Chem.* **1987**, *91*, 4779.

(30) (a) Nefedov, V. I.; Gati, D.; Dzhurinskii, B. F.; Sergushin, N. P.; Salyn, Y. V. *Zh. Neorg. Khim.* **1975**, *20*, 2307. (b) Atanassova, E.; Spassov, D. *Surf. Sci. Spectra* **2000**, *7*, 143. (c) Sarma, D. D.; Rao, C. N. R. *J. Electron Spectrosc. Relat. Phenom.* **1980**, *20*, 25.

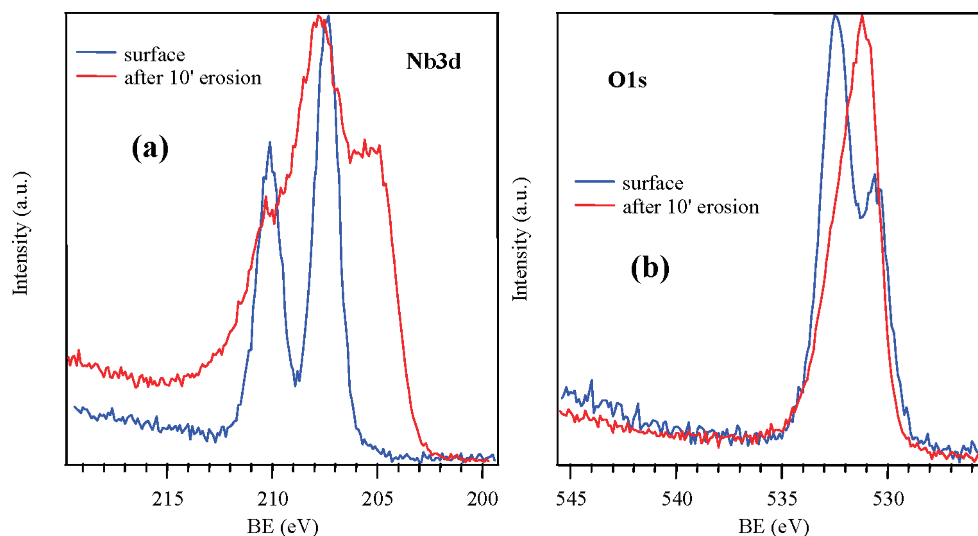

Figure 7. XPS spectra of (a) Nb 3d and (b) O 1s regions of an Nb_2O_5 thin film deposited at 600 °C from compound **1** by MOCVD.

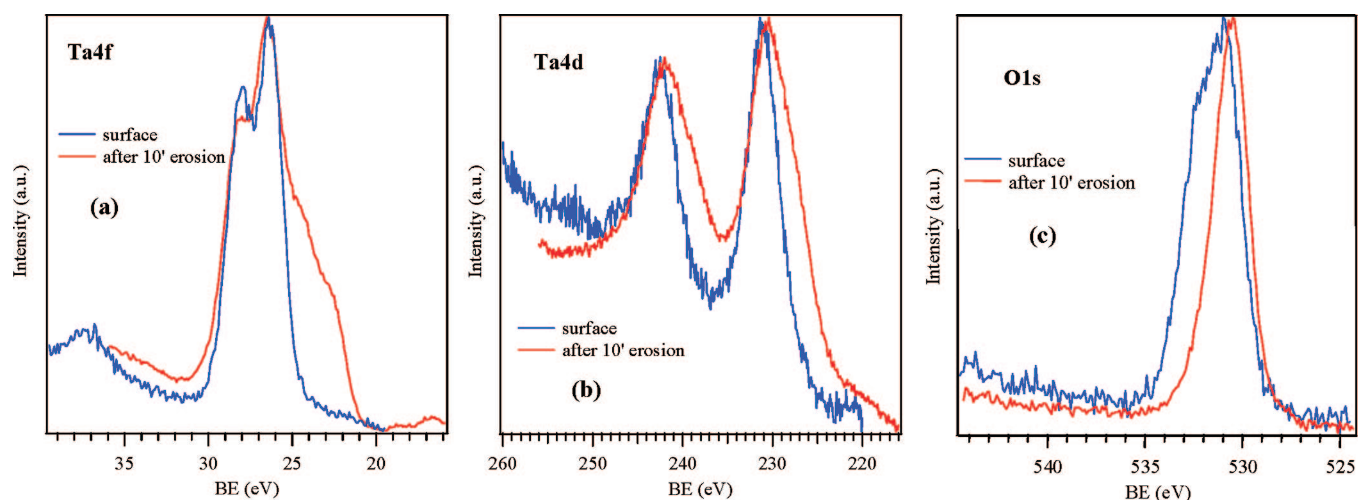

Figure 8. XPS spectra of (a) Ta 4f, (b) Ta 4d, and (c) O 1s regions of a Ta_2O_5 thin film deposited at 600 °C using compound **2** by LI-MOCVD.

layers and reasonably ascribed to contact with the outer atmosphere prior to XPS analyses. Correspondingly, the O/Nb atomic ratio was equal to 2.1, an appreciably lower value than the surface one, thus indicating a stoichiometry close to that of NbO_2. Such a phenomenon, corroborated by the apparent Nb reduction (see Figure 7a), was attributed to the concurrence of oxygen preferential sputtering[31] and to the loss of surface hydroxyls, clearly evidenced by marked variations in the O 1s band shape (see Figure 7b). After sputtering, carbon atomic percentage was reduced from 50.8 to 7.4 at. %, indicating that it mainly arose from atmospheric contamination.

In the case of Ta_2O_5, the high-BE shoulder at ≈531.9 eV was ascribed to surface –OH groups and underwent an appreciable intensity reduction after 10 min of sputtering (Figure 8). As in the case of Nb_2O_5, this phenomenon suggested that the hydration was limited to the outermost sample layers and can be ascribed to exposure to the outer atmosphere prior to the XPS analysis. After erosion, the O/Ta ratio was equal to 1.2 due to both O preferential sputtering and surface loss of hydroxyl groups. Correspondingly, carbon atomic percentage for Ta_2O_5 was reduced from 41.7 to 11.8 at. %, again indicating that it mainly arose from atmospheric contamination.

SNMS depth profiling was used to determine the film composition throughout the layer down to the interface to the substrate. Depth profiles of Nb, Ta, O, C, and N from the top surface of the films until the film–substrate interface are shown in Figure 9. In case of Nb_2O_5 films (grown at 600 °C), Nb concentration level of 24 at. % and O concentration of 63 at. % were obtained. In addition, the presence of about 6.5% of carbon and 6.5% of N could be detected. In the case of LI-MOCVD grown Ta_2O_5 films (grown at 600 °C) Ta concentration of 18% and O levels of 56% were obtained as shown in Figure 10. However, relatively higher content of C (12%) as well as N (10%) was obtained which could probably be due to the

(31) Choudhury, T.; Saied, S. O.; Sullivan, J. L.; Abbot, A. M. *J. Phys. D: Appl. Phys.* **1989**, *22*, 1185.
(32) Chiu, F.; Wang, J.; Lee, Y.; Wu, S. *J. Appl. Phys.* **1997**, *81*, 6911.
(33) Pignolet, A.; Rao, G. M.; Krupanidhi, S. B. *Thin Solid Films* **1995**, *261*, 18.
(34) Thomas, R.; Ehrhart, P.; Milanov, A.; Bhakta, R.; Baunemann, A.; Devi, A.; Fischer, R. A.; Waser, R. *J. Electrochem. Soc.* **2007**, *154*, G77.

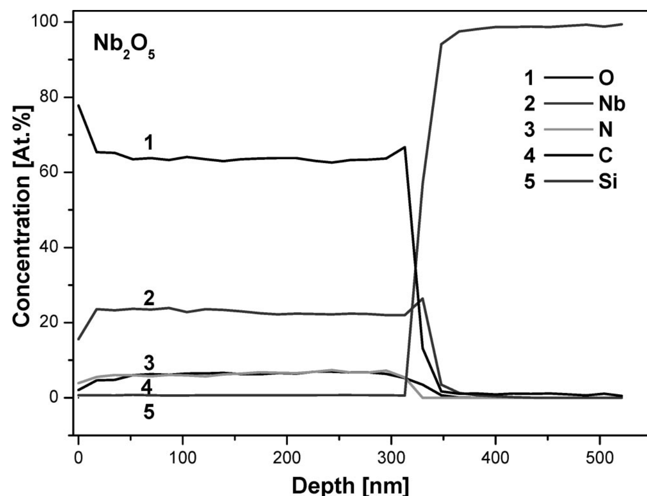

Figure 9. SNMS depth profile analysis of an Nb_2O_5 film deposited at 600 °C from compound **1** by MOCVD.

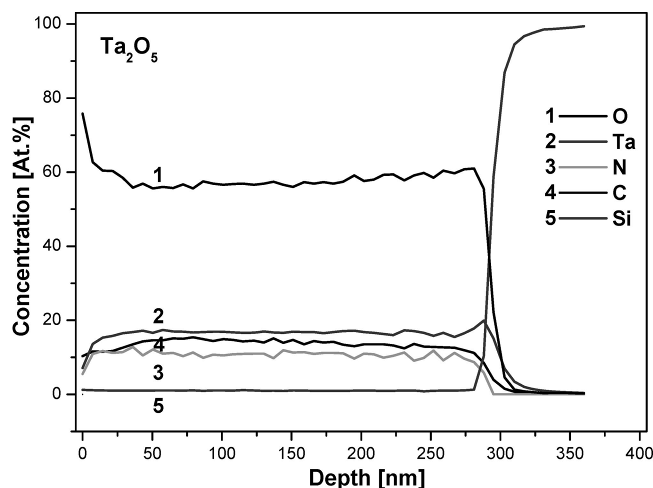

Figure 10. SNMS depth profile analysis of a Ta_2O_5 film deposited at 600 °C from compound **2** by LI-MOCVD.

decomposition of the solvent used in case of LI-MOCVD. This could be confirmed when comparing the SNMS data obtained on the MOCVD grown Ta_2O_5 film (at the same temperature) where the impurity content was lower (C: ~6%; N: ~6%) (Figure D of the Supporting Information). In both Nb_2O_5 and Ta_2O_5 films, the incorporation of N throughout the film thickness may be due to the presence of amide ligands in the precursor. It should be noted that similar levels of contamination (~5–10%) have been reported for films grown using mixed alkoxide–diketonates and metal alkylamides of these metals.[5a,14a,b] RBS analysis also was used as an additional technique for determining the film composition (details given in Figures E and F of the Supporting Information), and the results obtained were consistent with those obtained from XPS and SNMS.

The electrical characterization was carried out by measuring the *C*–*V* characteristics of the oxide films to investigate their suitability for potential application in metal–insulator–semiconductor (MIS) [(Pt/Nb_2O_5/SiO_x/Si and Pt/Ta_2O_5/SiO_x/Si)] capacitor structures for high-*k* application. Figure 11a,b shows the respective *C*–*V* curves at 100 kHz for Nb_2O_5 and Ta_2O_5 films grown at 600 °C. It should be noted here that the *C*–*V* measurements presented here are for the as-deposited films which were amorphous. In order to extract the relative dielectric permittivity, oxide films with higher thickness (~200–300 nm) were grown as this will reduce the effect of interlayer capacitance of the native SiO_x, which is around 2 nm, and hence the effective capacitance is almost equivalent to the capacitance of the high-*k* layer. From the measured C_{max} at accumulation, the relative dielectric permittivity calculated was around 27 and 24 for Nb_2O_5 (film thickness = 265 nm) and Ta_2O_5 (film thickness = 220 nm), respectively, which is in agreement with the range reported in literature for thin films of these materials.[32,33] CV curves presented in Figure 11 show counterclockwise hysteresis (ΔV_{fb} = 296 mV for Nb_2O_5 and ΔV_{fb} = 138 mV for Ta_2O_5) as the voltage swept from the positive to negative voltage and back. From the width, rechargeable oxide trap density in the film was estimated and was found to be around $2 \times 10^{11}/cm^2$ for Nb_2O_5 and $7 \times 10^{10}/cm^2$ for Ta_2O_5. The hysteresis in both cases can be reduced upon annealing,[34] and this was not considered in the present case as we were interested only in the dielectric constant of this type of material for high-*k* application. Leakage current through the complete gate stack was very low within the voltage ±2 V and was in the noise level (10^{-13} A) of the electrometer and hence not presented here.

Summary and Conclusions

Two new mixed dialkylamide–malonate complexes of Nb and Ta were synthesized in high yields and characterized in detail. The stabilization of the parent dialkylamide

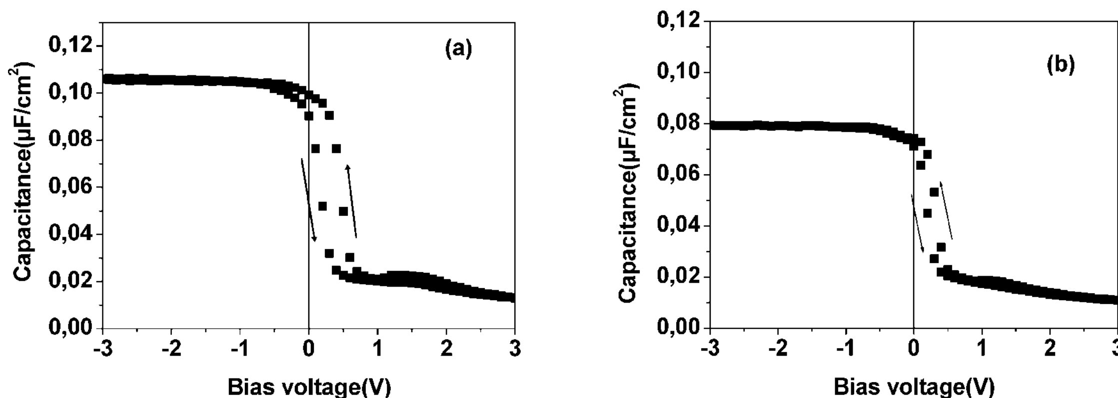

Figure 11. CV curves of (a) Nb_2O_5 grown MOCVD and (b) Ta_2O_5 films grown by LI-MOCVD.

complexes of Nb and Ta using bidentate malonates as chelating ligands reduces the high reactivity of the parent amide compounds by shielding the Lewis acidic center. The complexes are monomeric wherein the metal center is coordinated by four dimethlyamido groups and one chelating malonate ligand in a distorted octahedral geometry in the solid state. The compounds are solids at room temperature and showed enhanced thermal and chemical stability compared to their respective parent alkylamides. Thermal characterization results showed that both the compounds could be effectively used as precursors for CVD related applications. The high solubility and stability of this class of compounds makes them particularly interesting for LI-MOCVD as demonstrated in the case of Ta_2O_5. Thin films of Nb_2O_5 and Ta_2O_5 were successfully grown in the temperature range 400–800 °C by MOCVD. The Nb_2O_5 films crystallized around 700 °C whereas the crystallization temperature of Ta_2O_5 was as high as 800 °C. Surface roughness was dependent on the deposition temperature; at lower temperatures films were smoother due to the amorphous nature, and at higher temperatures the roughness increased as a result of crystalline grain growth. The deposition of uniform films over 3D structures was demonstrated. The presence of carbon and nitrogen was observed in the deposited films under the adopted CVD process conditions. Electrical properties of the films were quite encouraging in terms of high relative dielectric permittivity. Our current efforts are directed toward testing these precursors for ALD applications and also evaluating the compatibility of these compounds with other precursors (Ti, Sr, etc.) for the growth of complex oxides.

Acknowledgment. Financial support from the Deutsche Forschungsgemeinschaft (DFG, CVD-SPP-1119, DE-790/3-3) and the Italian Research Program FISR-MIUR “Inorganic and hybrid nanosystems for the development and innovation of fuel cells” is gratefully acknowledged. Dr. H. Parala is acknowledged for helpful discussions and for the critical comments on the manuscript.

Supporting Information Available: Figures of isothermal studies of compounds **1** and **2**, XRD analysis of Nb_2O_5 and Ta_2O_5 films, SEM, SNMS analysis, and RBS analysis of Nb_2O_5 and Ta_2O_5 films. This information is available free of charge via the Internet at http://pubs.acs.org.

CM0630441